

A bacterial toxin catalyzing tyrosine glycosylation of Rho and deamidation of G_q and G_i proteins

Thomas Jank¹, Xenia Bogdanović², Christophe Wirth², Erik Haaf³, Michael Spoerner⁴, Kira E Böhmer¹, Marcus Steinemann¹, Joachim H C Orth¹, Hans Robert Kalbitzer⁴, Bettina Warscheid^{3,5,6}, Carola Hunte^{2,6} & Klaus Aktories^{1,6}

Entomopathogenic *Photorhabdus asymbiotica* is an emerging pathogen in humans. Here, we identified a *P. asymbiotica* protein toxin (PaTox), which contains a glycosyltransferase and a deamidase domain. PaTox mono-O-glycosylates Y32 (or Y34) of eukaryotic Rho GTPases by using UDP-*N*-acetylglucosamine (UDP-GlcNAc). Tyrosine glycosylation inhibits Rho activation and prevents interaction with downstream effectors, resulting in actin disassembly, inhibition of phagocytosis and toxicity toward insects and mammalian cells. The crystal structure of the PaTox glycosyltransferase domain in complex with UDP-GlcNAc determined at 1.8-Å resolution represents a canonical GT-A fold and is the smallest glycosyltransferase toxin known. ¹H-NMR analysis identifies PaTox as a retaining glycosyltransferase. The glutamine-deamidase domain of PaTox blocks GTP hydrolysis of heterotrimeric $G_{\alpha_q/11}$ and G_{α_i} proteins, thereby activating RhoA. Thus, PaTox hijacks host GTPase signaling in a bidirectional manner by deamidation-induced activation and glycosylation-induced inactivation of GTPases.

Several bacterial protein toxins and effectors target host proteins by glycosylation in order to alter host cell functions such as immune-cell signaling, organization of the cytoskeleton, protein synthesis or apoptosis^{1,2}. Prototypes of glycosylating toxins are toxins A and B from *Clostridium difficile*, a pathogen causing antibiotic-associated diarrhea and pseudomembranous colitis³. The toxins glycosylate Rho proteins and inhibit Rho-dependent signaling. Effectors of the Lgt family of *Legionella pneumophila*, the cause of Legionnaires' disease, glycosylate eukaryotic elongation factor 1A, thereby inhibiting protein synthesis². So far, all these toxins and effectors modify target proteins by mono-O-glycosylation at threonine or serine residues. Notably, mono-O-glycosylation by eukaryotic enzymes occurs exclusively at serine and threonine residues. Accordingly, serine and threonine residues are sites for cytoplasmic or nuclear mono-O-glycosylation catalyzed by O-linked β -*N*-acetylglucosamine (O-GlcNAc) transferase⁴.

We set out to clarify the mode of action of a new bacterial protein toxin, PaTox, from *P. asymbiotica*, which has been recognized as an emerging human pathogen⁵. *Photorhabdus* species are known as luminescent entomopathogenic bacteria, which are mutualistically associated with soil nematodes of the genus *Heterorhabditis*⁶. The nematodes harbor *Photorhabdus* bacteria in their intestine and invade insect larvae, where they release the bacteria⁷. Upon contact with the insect hemocoel, *Photorhabdus* release several protein toxins. The toxins inhibit insect immune responses and eventually kill the insect larvae⁷. The remaining cadaver functions as a nutrition source for

proliferation of nematodes and bacteria. Among the genus *Photorhabdus*, *P. asymbiotica* is apparently the only pathogen affecting humans, causing invasive soft-tissue and disseminated bacteremic infections^{8,9}. *P. asymbiotica* was first described as a nonsymbiotic strain⁵ but was later found to be associated with nematodes as well¹⁰. Genome analysis revealed that *P. asymbiotica* acquired virulence factors from diverse human pathogens, including *Salmonella* and *Yersinia* species, which are not found in other *Photorhabdus* species¹¹.

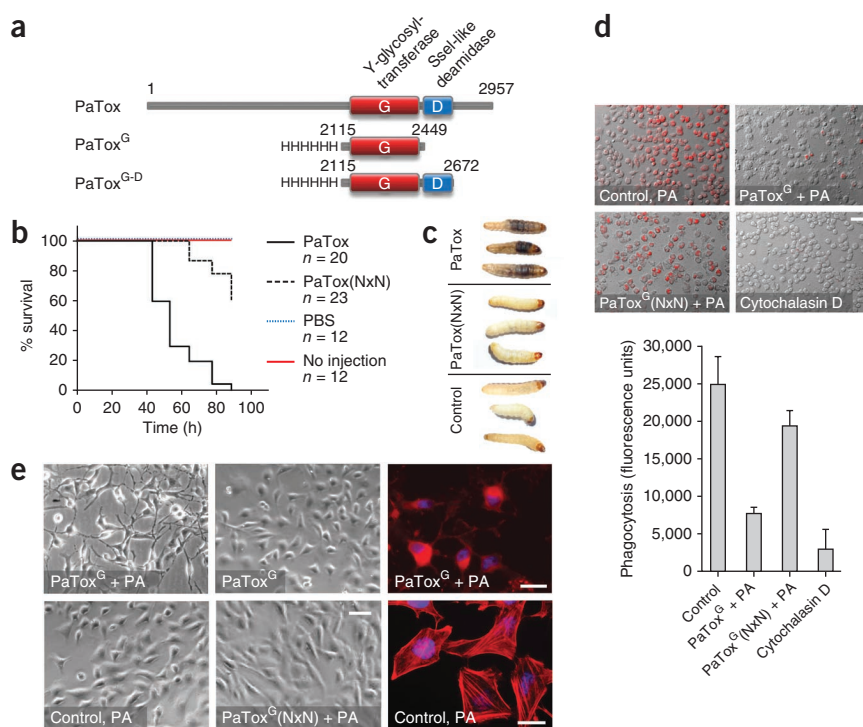
Accordingly, PaTox contains a C-terminal region exhibiting sequence similarity with the *Salmonella* effector SseI (also known as SrfH). SseI is translocated into host cells by the type III secretion system SPI-2 and seems to be involved in control of host immune-cell migration^{12,13}. Although the crystal structure of *Salmonella* SseI was reported, showing similarity with deamidases, the enzyme activity of SseI remained unclear¹⁴.

We report that the glycosyltransferase activity of PaTox modifies Rho GTPases by tyrosine mono-O-glycosylation to result in inhibition of Rho signaling. The SseI-like domain activates heterotrimeric G_{α} proteins by deamidation, thereby activating small Rho GTPases through G_{α_q} and $G_{\alpha_{11}}$ ($G_{\alpha_{q/11}}$). Activation of Rho appears to be a prerequisite for mono-O-glycosylation. Tyrosine glycosylation of Rho inhibits downstream signaling by an impaired interaction with diverse regulator and effector proteins of Rho and, eventually, leads to actin disassembly, blockade of phagocytosis and insect-host and mammalian-cell death.

¹Institut für Experimentelle und Klinische Pharmakologie und Toxikologie, Albert-Ludwigs-Universität Freiburg, Freiburg, Germany. ²Institut für Biochemie und Molekularbiologie, Albert-Ludwigs-Universität Freiburg, Freiburg, Germany. ³Zentrum für Biosystemanalyse, Albert-Ludwigs-Universität Freiburg, Freiburg, Germany. ⁴Institut für Biophysik und Physikalische Biochemie, Universität Regensburg, Regensburg, Germany. ⁵Institut für Biologie II, Fakultät für Biologie, Albert-Ludwigs-Universität Freiburg, Freiburg, Germany. ⁶Centre for Biological Signalling Studies (BIOSS), Albert-Ludwigs-Universität Freiburg, Freiburg, Germany. Correspondence should be addressed to K.A. (klaus.aktories@pharmakol.uni-freiburg.de).

Received 28 May; accepted 11 September; published online 20 October 2013; doi:10.1038/nsmb.2688

Figure 1 PaTox and toxic effects. **(a)** Schematic of PaTox with the tyrosine-glycosyltransferase domain (G) and the domain with similarity to virulence factor SseI from *Salmonella* (D) and histidine-tagged fragments PaTox^G and PaTox^{G-D} used in this study. **(b)** Kaplan–Meier survival plot of *G. mellonella* injected with full-length PaTox, inactive PaTox(NxN) or phosphate-buffered saline (PBS), or not injected (*n*, number of individuals). Similar results were obtained from another independent experiment. **(c)** Pictures of *G. mellonella* from **b** 53 h after injection. **(d)** Fluorescence and Nomarski microscopy of phagocytosis of fluorescently labeled *E. coli* particles by J774 macrophages treated with PaTox^G or PaTox^{G(NxN)} mutant, with anthrax protective antigen (PA) as a delivery system. Cytochalasin D, which causes depolymerization of actin, is a positive control. Top, overlay of microscopy images; bottom, quantification of phagocytosis by fluorescence spectroscopy (means \pm s.d. from three technical replicates). **(e)** Nomarski (left) and fluorescence (right) microscopy to assess the effects of PaTox^G on the actin cytoskeleton. HeLa cells were treated with PaTox^G or inactive PaTox^{G(NxN)} without and with PA as a delivery system. Right, actin was stained with tetramethylrhodamine isothiocyanate (TRITC)-phalloidin and nuclei with 4',6-diamidino-2-phenylindole (DAPI). Scale bars, 50 μ m (**d** and **e**, left) or 10 μ m (**e**, right).



RESULTS

PaTox is a glycosyltransferase

Using basic local alignment search tool (BLAST)-based analyses, we identified sequence motifs in *P. asymbiotica* known from glycosylating toxins in *Clostridium* and *Legionella* (**Supplementary Fig. 1a**)². The toxin sequences are characterized by an aspartic acid–X–aspartic acid (DxD) motif important for the coordination of a divalent cation and for nucleotide-sugar binding¹⁵. The gene identified encoded a putative protein toxin of 2,957 amino acids with a proposed glycosyltransferase domain in the C terminus containing an extended DxDD motif (**Fig. 1a**). We found a region downstream of this domain that exhibited ~68% sequence similarity with the *Salmonella* virulence factor SseI, whose function is unknown¹⁴. We could not recognize other substantial sequence similarities.

From *P. asymbiotica*, isolated from a patient's leg wound⁸, several fragments of the toxin were cloned (**Fig. 1a**), expressed in *Escherichia coli* and purified as histidine-tagged proteins. In order to analyze the toxicity of PaTox, we injected full-length protein into the hemocoel of *Galleria mellonella* (greater wax moth) larvae (**Fig. 1b,c**). Within 53 h, a strong dorsal melanization appeared, and all toxin-treated insect larvae died after 88 h. When we changed the DxD motif of the glycosyltransferase domain to asparagine–X–asparagine (NxN) by mutagenesis, no significant melanization of the larvae occurred, and 61% of the larvae survived, thus indicating a crucial function of the putative glycosyltransferase in toxicity. Because *Photothabdus* inhibits the innate immune system of the host^{16,17}, we studied the effect of the putative glycosyltransferase domain (PaTox^G) on phagocytosis by mammalian J774 macrophages. Therefore, we introduced purified PaTox^G into macrophages, using protective antigen (PA), the component of anthrax toxin responsible for binding and translocation, as a delivery system^{18,19}. PaTox^G strongly blocked phagocytosis of fluorescently labeled *E. coli* particles (**Fig. 1d**). By contrast, when we changed the DxD motif of PaTox^G to NxN by mutagenesis, the

antiphagocytic effect was blocked. An intact actin cytoskeleton is crucial for phagocytic activity. Therefore, we studied the effects of PaTox^G on the actin cytoskeleton of HeLa cells, using PA as a delivery system. PaTox^G induced major morphological changes and disassembly of actin filaments (**Fig. 1e**). Again, the NxN mutant of PaTox^G was without cytotoxic effects (**Fig. 1e**), results suggesting the essential role of a glycosyltransferase activity.

PaTox^G modifies a tyrosine residue of Rho GTPases

To identify the cellular substrate of PaTox, we incubated mammalian macrophage (J774 cell) extracts with PaTox^G and various radiolabeled UDP sugar donors. Subsequent SDS-PAGE analysis revealed radioactively labeled proteins with molecular masses of ~23 kDa in the presence of UDP-[¹⁴C]GlcNAc but not with UDP-[¹⁴C]galactose or UDP-[¹⁴C]glucose (**Fig. 2a**). We confirmed sugar-donor specificity by determination of the UDP-GlcNAc hydrolase activity of PaTox^G (**Supplementary Fig. 1c**). [¹⁴C]GlcNAc-modified proteins migrated similarly in SDS-PAGE (**Fig. 2a**) to Rho GTPases, which are key regulators of the actin cytoskeleton. Therefore, we tested several small GTPases as substrates in *in vitro* glycosylation (**Fig. 2b**). These studies revealed toxin-induced GlcNAcylation of RhoA, RhoB, RhoC, Rac1, Rac2, Rac3 and Cdc42. By contrast, other GTPases of the Rho, Ras or Rab families were not modified. Glycosylation strictly depended on the DxD motif of PaTox^G. An NxN mutant was inactive (**Supplementary Fig. 1d**). Thus, PaTox was a highly donor-specific and acceptor-selective glycosyltransferase.

To disclose the glycosyl-acceptor residue in Rho modified by PaTox^G, we applied tandem-MS analyses but were initially not able to identify the modification by looking for conventional acceptor amino acids as glycosyl acceptors (serine, threonine and asparagine). We included unconventional glycosyl-acceptor amino acids (tyrosine, tryptophan and arginine) in the search algorithm and found that Y34 of RhoA and the equivalent Y32 of Rac and Cdc42 were covalently

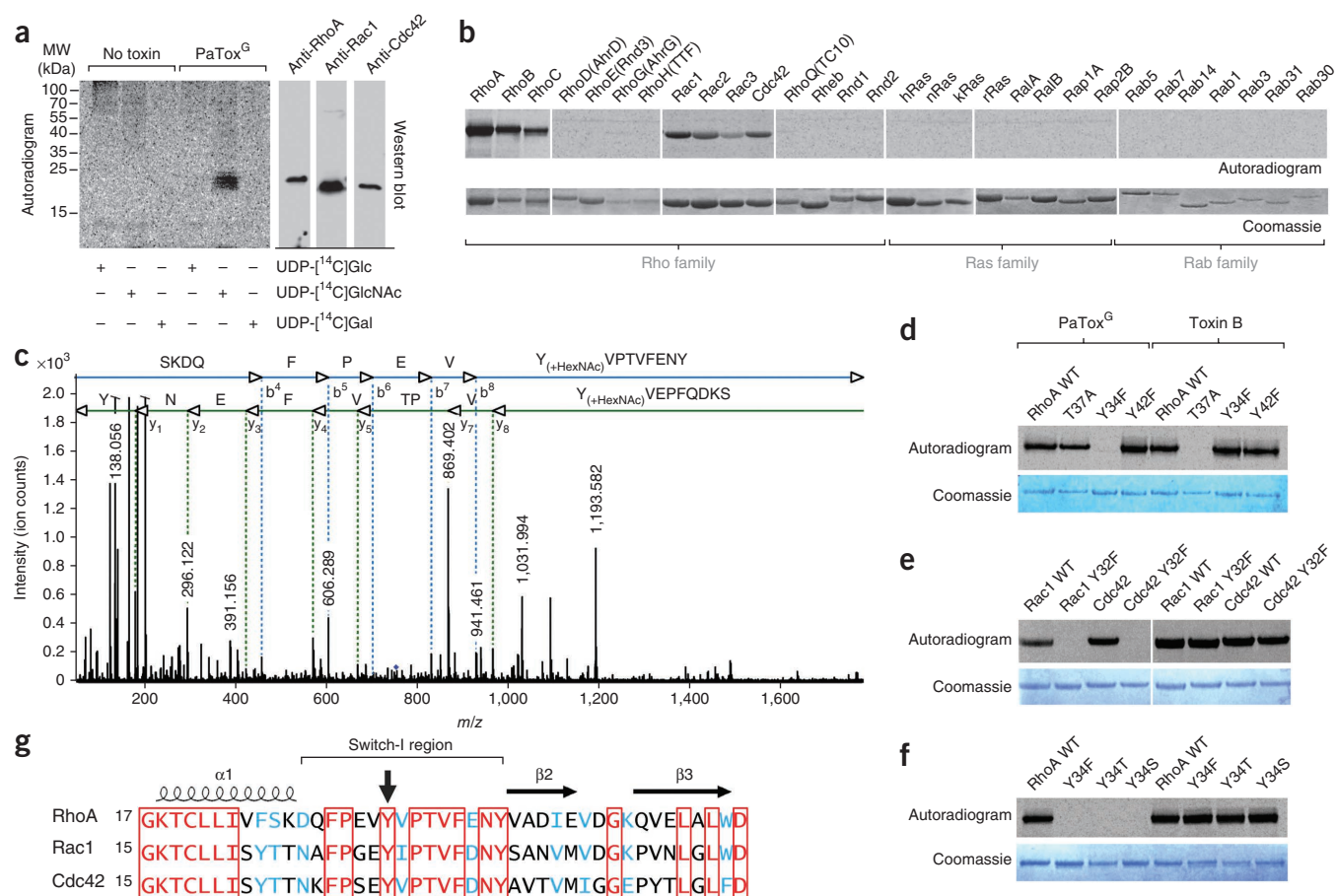


Figure 2 *Photorhabdus* glycosyltransferase GlcNAcylates Rho GTPases at a tyrosine residue. (a) Left, autoradiogram of SDS-PAGE from macrophage (J774 cell) lysate incubated with and without PaTox^G in the presence of ¹⁴C-labeled UDP sugars (Glc, glucose; GlcNAc, *N*-acetylglucosamine; Gal, galactose). MW, molecular weight. Right, western blot analysis with the indicated antibodies. (b) Autoradiogram and Coomassie staining of SDS-PAGE to assess substrate specificity of PaTox. Rho-, Ras- and Rab-family proteins were *in vitro* glycosylated by PaTox^G with UDP-[¹⁴C]GlcNAc. (c) MS/MS analysis of PaTox-modified RhoA, identifying Y34 as acceptor amino acid. Sequence-specific fragment ions are annotated in blue (b-type ions) or green (y-type ions). *m/z*, mass/charge ratio. (d–f) Autoradiograms and Coomassie stainings of *in vitro* ¹⁴C-GlcNAcylated wild-type (WT) RhoA (d,f), Rac1, Cdc42 (e) and indicated mutants by PaTox^G. *C. difficile* toxin B, which glycosylates T37 of RhoA, was used as a control with UDP-[¹⁴C]glucose. (g) Amino acid sequence alignment of Rho GTPases in the region of the switch I loop. The GlcNAc-acceptor tyrosine is marked with an arrow. The alignment was prepared with Clustal W and ESPript 2.2 (<http://esprict.ibcp.fr>). Identical residues are boxed and shown in red, and similar residues are in blue. Full-length images of gels, immunoblots and autoradiographs are shown in **Supplementary Figure 6**.

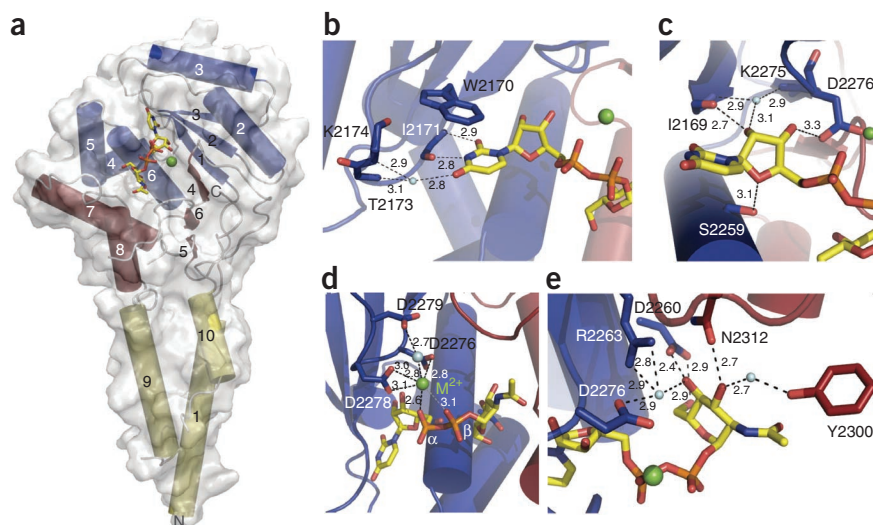
modified by *N*-acetyl hexosamine (Fig. 2c,d and **Supplementary Fig. 2**). We verified the modification at these tyrosine residues by mutational studies (Fig. 2d,e). Exchange of Y32 (or Y34) in RhoA, Rac and Cdc42 with phenylalanine prevented glycosylation by PaTox^G, whereas glycosylation with *C. difficile* toxin B, which modifies Rho proteins at T37 (RhoA) and T35 (Rac and Cdc42)²⁰, was still possible. Conversely, change of T37 of RhoA to alanine prevented modification by *C. difficile* toxin B, whereas GlcNAcylation by PaTox^G remained unchanged. For a control, we changed Y42 of RhoA to phenylalanine. This mutation did not affect glycosylation by PaTox^G or by toxin B (Fig. 2d). Moreover, exchange of Y34 in RhoA with serine or threonine prevented modification by PaTox^G, thus indicating that the new type of modification is highly specific for tyrosine (Fig. 2f).

To study whether the modification of Rho proteins occurs during the infection process, we infected insect Sf9 cells with *P. asymbiotica* and *Photorhabdus luminescens* for 14 h. We could show that glycosylation at the switch I tyrosine residue of Rho was only found in *P. asymbiotica*-infected cells but not in cells infected with *P. luminescens*, which lacked the gene encoding PaTox (**Supplementary Fig. 2e,f**).

Crystal structure of PaTox^G

In order to gain insights into the structural basis of PaTox-induced tyrosine glycosylation, we crystallized and determined the X-ray structure of PaTox^G in complex with UDP-GlcNAc at 1.8-Å resolution (Fig. 3a, Table 1 and **Supplementary Fig. 3a,b**). The obtained structure showed a remarkably small protein glycosyltransferase with a cone-like shape comprising a globular catalytic head and a three-helix bundle. The glycosyltransferase domain revealed a Rossmann-like fold with a central six-stranded β-sheet sandwiched by α-helices on both sides. UDP-GlcNAc was bound by several residues in the enzyme's active site (Fig. 3b–e). Thereby, U nucleoside was tightly bound, with the base moiety stabilized by aromatic stacking and with all possible hydrogen bond positions satisfied, thus providing specificity for the nucleoside (Fig. 3b,c). The divalent cation was coordinated by the pyrophosphate of UDP and the carboxylate groups of the extended DxDD motif (Fig. 3d). The GlcNAc moiety was specifically bound by direct and water-mediated hydrogen bond interactions exposing the anomeric C1 atom to the solvent (Fig. 3e). Several amino acids involved in UDP-GlcNAc interaction were conserved, and their exchange reduced

Figure 3 Crystal structure of PaTox^G. (a) Three-dimensional structure of PaTox^G with UDP-GlcNAc (yellow) bound to the active center. α -helices and β -strands are numbered consecutively. (b–e) Close-up views of the UDP-GlcNAc-binding site of PaTox^G. Side chains involved in UDP-GlcNAc (yellow) binding are shown as sticks and a divalent metal ion (M^{2+}) as a green sphere. (b) Aromatic stacking of the nucleotide base with the side chain of W2170. Base specificity is conferred by two hydrogen bonds with backbone atoms of I2171 and a water-mediated hydrogen bond to T2173 and K2174. (c) Stabilization of the ribose moiety by the side chains of S2259 and D2276, the backbone nitrogen atom of I2169 and a water molecule. (d) Interactions of the extended DxDD motif. Cocrystallized Ca^{2+} (M^{2+}) is coordinated by oxygen atoms of both phosphate groups, the carboxylate groups of the extended DxDD motif (D2276-x-D2278-D2279) and a water molecule. (e) Stabilization of the GlcNAc moiety by direct and water-mediated hydrogen bonds of N2312, D2260, R2263 and Y2300.



transferase activity dramatically in the case of W2170A, D2260A and R2263A (**Supplementary Table 1**). We obtained corroborating results when we applied the mutants PaTox^G-D2260A and PaTox^G-D2263A to cell intoxication experiments (**Supplementary Fig. 3c**). Notably, mutation of the residues of the extended DxDD motif D2276N, D2278N and D2279N strongly affected tyrosine glycosylation of RhoA (**Supplementary Table 1**).

The structure clearly assigned PaTox^G to the glycosyltransferase GT-A family. Despite negligible sequence similarity, the catalytic domain revealed a similar structure to toxin glycosyltransferases from *Clostridium* spp. and *Legionella* (**Supplementary Table 2**). All of these structures have substantial insertions, particularly in the acceptor-binding fold. Furthermore, structural homology was high for SpsA, the prototype of GT-A enzymes, and to glycogenin. The analysis showed that the catalytic domain of PaTox^G exhibits the smallest known structure for glycosyltransferase toxins and represents the canonical GT-A fold (**Supplementary Fig. 3b**).

Functional consequences of tyrosine GlcNAcylation

In Rho proteins, the glycosyl acceptor Y32 (or Y34) is located in the switch I region (residues 28–42), which rearranges between the GDP- and GTP-bound form of the GTPases (**Supplementary Fig. 4a,b**). However, GlcNAcylation did not alter the binding of fluorescently labeled *N*-methylantraniloyl (mant)-GDP (**Supplementary Fig. 4c**) and mant-GppNHp (**Supplementary Fig. 4d**), a nonhydrolyzable GTP analog, to RhoA.

In general, Rho proteins are regulated by a GTPase cycle (**Fig. 4a**)²¹. G nucleotide-exchange factors (GEFs) induce GDP-to-GTP exchange and thereby activate GTPases. In the active conformation, Rho proteins interact with effector proteins, which promote downstream signaling. Inactivation of Rho is mediated by GTPase-activating proteins (GAPs), which accelerate GTP hydrolysis. We studied the steps of the GTPase cycle, which were affected by PaTox-induced modification. Tyrosine GlcNAcylation strongly blocked the activation of RhoA by leukemia-associated RhoGEF (LARG) (**Fig. 4b**), PDZ-RhoGEF (**Supplementary Fig. 4e**) and p47-LBC GEF (**Supplementary Fig. 4f**). To study RhoA-effector interaction, we pretreated HeLa cells with PaTox^G in the presence of PA and, for comparison, with Rho-inhibiting toxin B²⁰ or the Rho-activating cytotoxic necrotizing factor (CNF)²². Thereafter, we stimulated Rho activity by addition

of serum to the cell medium. Pulldown experiments with the Rho-binding domain of the effector Rhotekin (**Fig. 4c**) revealed inhibition of RhoA-Rhotekin interaction by PaTox^G and toxin B, whereas in mock and CNF-treated cells RhoA was precipitated by Rhotekin beads. Also, *in vitro* studies with recombinant RhoA, Rac and Cdc42 and the effectors Rhotekin and PAK showed that toxin-induced GlcNAcylation blocked interaction of Rho proteins with their effectors

Table 1 Data collection and refinement statistics

	PaTox ^G -UDP-GlcNAc	PaTox ^G SeMet
Data collection^a		
Space group	<i>C2</i>	<i>C2</i>
Cell dimensions		
<i>a</i> , <i>b</i> , <i>c</i> (Å)	145.82, 42.13, 116.37	145.80, 41.87, 113.98
α , β , γ (°)	90.0, 99.52, 90.0	90.0, 99.6, 90.0
		<i>Peak</i>
Wavelength	1.0000	0.9782
Resolution (Å) ^b	57.38–1.80 (1.90–1.80)	60.00–1.80 (1.90–1.80)
<i>R</i> _{merge}	0.17 (2.30)	0.17 (2.61)
<i>I</i> / σ <i>I</i>	7.6 (1.1)	18.2 (2.9)
Completeness (%)	98.8 (98.5)	92.9 (87.9)
Redundancy	8.6 (7.8)	5.7 (5.3)
Refinement		
Resolution (Å)	56.92–1.80	
No. reflections	61,067 (4,431)	
<i>R</i> _{work} / <i>R</i> _{free}	0.22 / 0.26	
No. atoms		
Protein	4,462	
Ligand	78	
Water	208	
<i>B</i> factors		
Protein	31.23	
Ligand	31.82	
Water	35.00	
r.m.s. deviations		
Bond lengths (Å)	0.009	
Bond angles (°)	1.285	

^aFor each data set, one crystal was measured. SeMet, selenomethionine. ^bValues in parentheses are for highest-resolution shell.

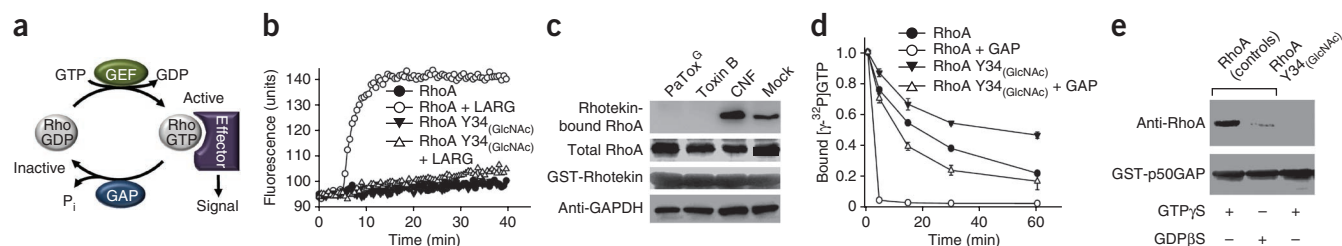


Figure 4 Functional consequences of RhoA GlcNAcylation at Y34. **(a)** Rho GTPase cycle. GDP-bound Rho is inactive. Nucleotide exchange by GEF activates Rho. Active, GTP-bound Rho interacts with endogenous effectors. GAPs inactivate Rho by facilitating GTP hydrolysis. P_i , inorganic phosphate. **(b)** Nucleotide exchange induced by RhoGEF LARG. Fluorimetric analysis of mant-GDP nucleotide exchange with wild-type RhoA or GlcNAcylated RhoA; RhoGEF LARG was added or not after 5 min. Data are representative of two independent experiments. **(c)** Western blot analysis of Rho-effector interaction. RhoA pull-down with Rhotekin-coupled beads from HeLa cells treated with PaTox^G (plus PA for delivery), *C. difficile* toxin B or cytotoxic necrotizing factor (CNF), or left untreated (mock), after serum stimulation. Bound RhoA was detected by anti-RhoA antibody. Immunoblots of total RhoA and GAPDH are shown as loading controls. Data are representative of three independent experiments. Full-length western blots are shown in **Supplementary Figure 7a**. **(d)** Time course of [γ -³²P]GTP hydrolysis by wild-type RhoA or GlcNAcylated RhoA, incubated without or with p50Rho-GAP. Remaining RhoA-bound GTP is shown relative to initial loading (mean \pm s.d.; $n = 3$ technical replicates). **(e)** Western blot of glutathione S-transferase (GST)-p50GAP-RhoA interaction. Wild-type and GlcNAcylated RhoA were preloaded with GTP γ S or GDP β S. Full-length blots are shown in **Supplementary Figure 7b**.

(**Supplementary Fig. 4g**). Finally, PaTox^G strongly inhibited GAP (p50Rho-GAP)-stimulated GTPase activity of RhoA (**Fig. 4d**). Accordingly, the toxin blocked the direct interaction of Rho-GAP with GlcNAcylated RhoA (**Fig. 4e**).

In order to find the basis of impaired effector and regulator interaction, we followed PaTox^G-mediated glycosylation of RhoA by ¹H-NMR measurements and found that changes caused by GlcNAcylation were restricted to Y34 only and did not alter the arrangement of the switch I region (**Fig. 5a**). This suggested that the attached GlcNAc residue impaired effector and regulator interaction, probably by steric hindrance.

PaTox^G is a retaining glycosyltransferase

To clarify the stereochemistry of the glycosyl-transfer reaction, we performed ¹H-NMR spectroscopy of tyrosine-GlcNAcylated RhoA. We obtained a resonance of H1' of the protein-bound GlcNAc as a doublet at 5.49 p.p.m. and determined a J -coupling value of 3.4 Hz, which was consistent with a sugar covalently attached in the α -anomeric configuration to the hydroxyl of Y34 (**Fig. 5b,c**). This revealed that PaTox was highly

stereospecific and transferred the sugar with net retention of the configuration of the anomeric C1' position with respect to the donor substrate. Thus, we could assign PaTox to the family of retaining glycosyltransferases.

Ssel-like domain of PaTox deamidates G α proteins

By analyzing the preferred nucleotide-binding state of Rho for tyrosine GlcNAcylation, we observed that RhoA loaded with the GTP analog GTP γ S or GppNHp was readily glycosylated, whereas GDP or GDP β S-loaded Rho was poorly modified (**Supplementary Fig. 4h,i**).

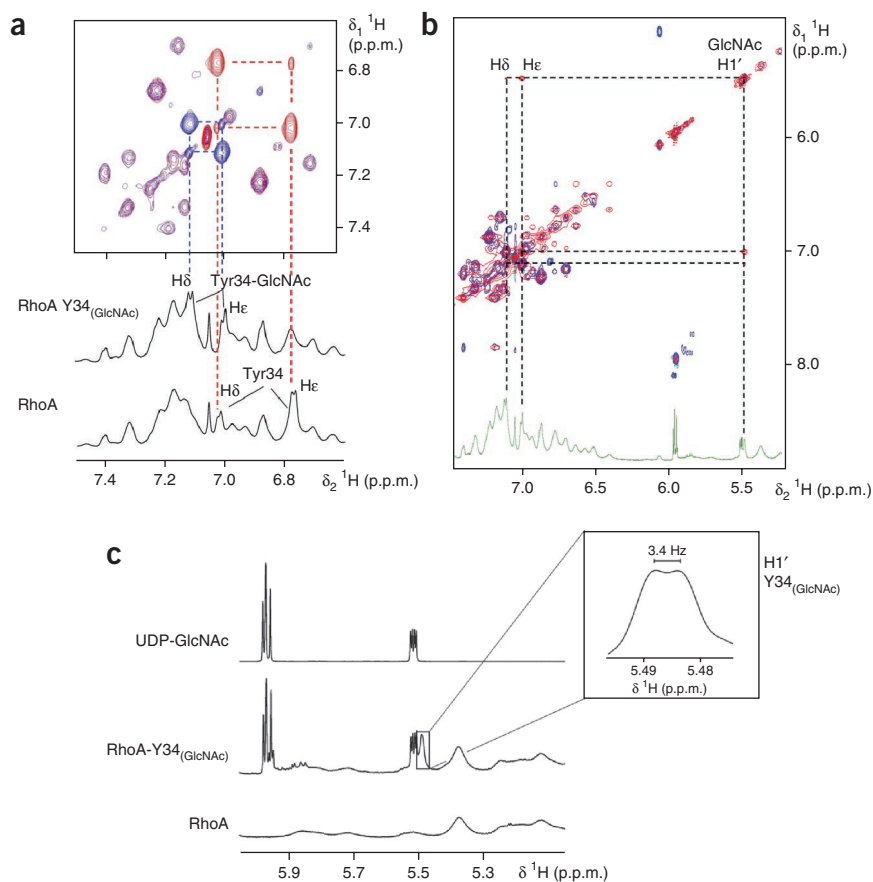
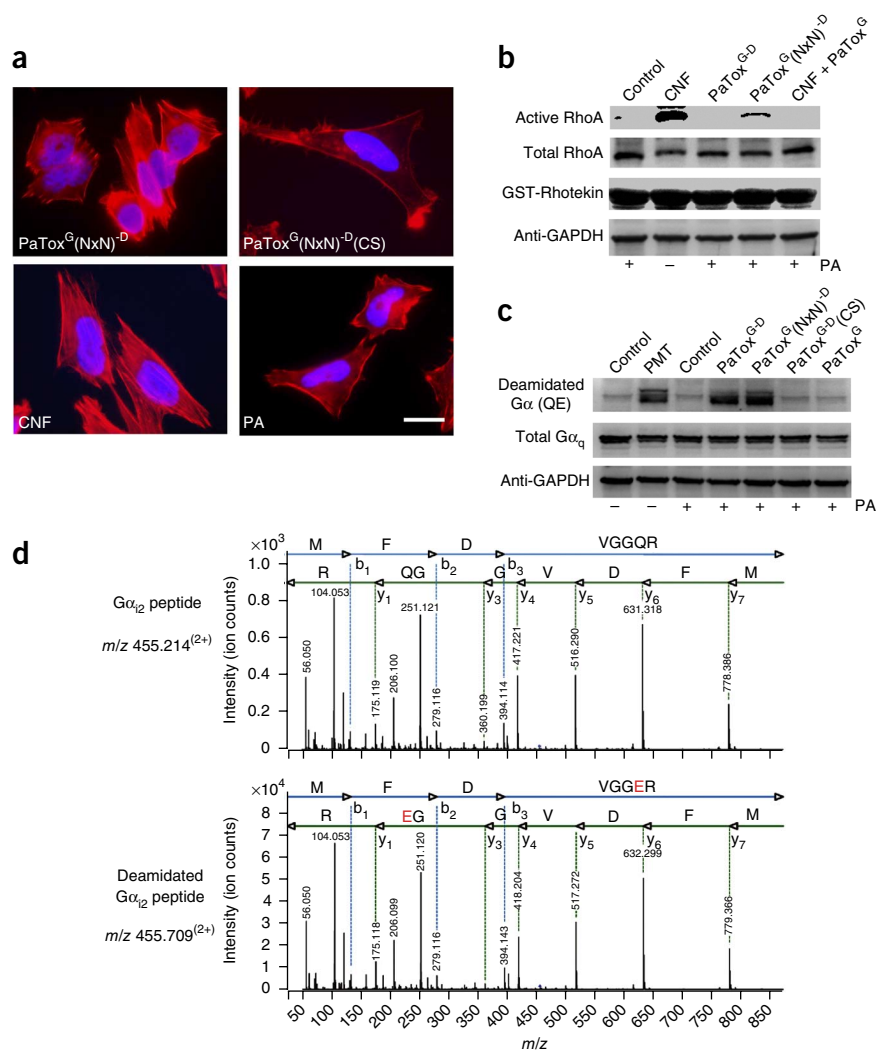


Figure 5 ¹H-NMR analysis of GlcNAc-modified RhoA. **(a)** Superposition of ¹H-TOCSY spectra of native RhoA (red) and RhoA modified by PaTox^G (blue) together with the corresponding ¹H 1D NMR spectra of native and modified RhoA. The spectral changes observable are restricted to Y34 only. **(b)** Superposition of ¹H-NOESY (red) and ¹H-TOCSY (blue) spectra of modified RhoA. The cross-signals from H δ and H ϵ of Y34 to the H1' of protein-bound GlcNAc (5.49 p.p.m.) are indicated. **(c)** Detail of the ¹H 1D spectra of native and modified RhoA. The zoom view shows the resonance of H1' of the protein-bound GlcNAc after application of a Gaussian filter. The doublet at 5.49 p.p.m. was fitted by a Gaussian function and provides a J -coupling value of 3.4 ± 0.5 Hz (digital resolution during data acquisition).

Figure 6 The SseI-like domain of PaTox deamidates heterotrimeric G α proteins. **(a)** Fluorescence micrographs of HeLa cells treated with PaTox^{G(NxN)^{-D}} (glycosyltransferase inactive and deamidase active) or PaTox^{G(NxN)^{-D}(CS)} (glycosyltransferase inactive and deamidase inactive) and PA as a delivery system after cell starvation. Rho-activating CNF and PA alone are controls. Actin and nuclei were stained by TRITC-phalloidin and DAPI, respectively. Scale bar, 10 μ m. Data are representative of three independent experiments. **(b)** RhoA activation by PaTox. Western blot of RhoA precipitation by GST-Rhotekin pull-down on HeLa cells treated with the indicated proteins with or without PA. Total RhoA, GST-Rhotekin and GAPDH are loading controls. Data are representative of two independent experiments. Uncropped blots are shown in **Supplementary Figure 7c**. **(c)** Western blot analysis of toxin-induced deamidation of heterotrimeric G α proteins in HeLa cells treated with the indicated proteins, using the monoclonal deamidation-specific antibody anti-G α QE (3G3). Immunoblots of total G α_q and GAPDH are input controls. Data are representative of three independent experiments. Uncropped blots are shown in **Supplementary Figure 7d**. **(d)** MS/MS analysis of PaTox-catalyzed deamidation of G α_{12} at Q205. MS/MS spectra of the tryptic peptide 199-MFDVGGQR-206 (top) and its deamidated form 199-MFDVGGER-206 (bottom) of G α_{12} observed at m/z 455.214⁽²⁺⁾ and m/z 455.709⁽²⁺⁾, respectively.



This was in contrast to glucosylation of RhoA by toxin B at T37, a modification that occurs preferentially with GDP-bound GTPases (**Supplementary Fig. 4h**)²⁰. Because under basal conditions the major cellular fraction of Rho is in the inactive GDP conformation, we were surprised to find that the GlcNAc transferase-deficient fragment PaTox^{G(NxN)^{-D}}, which contains the functional SseI-like domain (D), induced strong formation of stress fibers, a result indicating RhoA activation (**Fig. 6a**). Thus, we assumed that stress-fiber formation depended on the SseI-like domain.

The SseI-like domain exhibits sequence similarity with papain-like proteases and ~20% identity to the deamidase domain of *Pasteurella multocida* toxin (PMT) (**Supplementary Fig. 1b**). PMT activates heterotrimeric G proteins by deamidating a glutamine residue essential for GTP hydrolysis²³. The deamidase activity of PMT depends on a catalytic triad of cysteine, histidine and aspartic acid, which is also conserved in the SseI-like domain of PaTox (**Supplementary Fig. 1b**). When we additionally changed the equivalent catalytic cysteine (C2509 in PaTox) to serine in the SseI-like domain (to form PaTox^{G(NxN)^{-D}(CS)}), stress-fiber formation was blocked (**Fig. 6a**). Moreover, pull-down experiments with the Rho effector Rhotekin revealed that the glycosyltransferase-deficient mutant PaTox^{G(NxN)^{-D}}, which contained the SseI-like domain, caused activation of RhoA and interaction with Rhotekin (**Fig. 6b**). We used CNF as a control, which directly activates Rho proteins by deamidation of Q61 (or Q63). Again, tyrosine GlcNAcylation by PaTox^G was dominant and blocked activation of RhoA by CNF. MS analyses revealed that RhoA, Rac1 and Cdc42 were not deamidated by PaTox^{G-D}. To test whether PaTox^{G-D} possessed a deamidase activity similar to that of PMT, we used a

monoclonal antibody that selectively recognized the deamidation of a crucial glutamine residue in the switch II region of heterotrimeric G proteins²⁴. This antibody recognizes deamidation of G α subunits by PMT and reacted with G α subunits after treatment of cells with PaTox^{G-D} (**Fig. 6c**). By contrast, when we changed C2509 to serine (to form PaTox^{G-D}(CS)), deamidation was impaired. The antibody interaction occurred with PaTox^{G-D} containing the active or inactive GlcNAc transferase domain. We further analyzed purified α subunits of G β_1 , G β_3 , G β_4 , G β_{11} , G β_{12} , G β_{13} and G β_q . These studies revealed that, under the conditions used, PaTox^{G-D} deamidated only G α_i , G α_q and G α_{11} (**Supplementary Fig. 5a**). To prove deamidation of heterotrimeric G proteins, we performed MS analysis with PaTox^{G-D}-treated G α_i and identified deamidation of Q205 (**Fig. 6d**). This glutamine residue is conserved throughout the G α superfamily and is involved in GTP hydrolysis, thereby terminating the active state of the GTPase²⁵. Deamidation of the pivotal glutamine residue results in an inhibition of the GTPase activity and arrests the G protein in a permanent active state. It is known that the G α_{12} and G α_{13} (G $\alpha_{12/13}$) and G $\alpha_{q/11}$ families are capable of activating RhoA through GEFs such as p115RhoGEF and p63RhoGEF, respectively. To identify the G protein responsible for Rho activation by PaTox, we used G $\alpha_{q/11}$ - and G $\alpha_{12/13}$ -deficient mouse embryonic fibroblasts (MEFs) and analyzed PaTox^{G(NxN)^{-D}}-induced stress-fiber formation (**Supplementary Fig. 5b**). Only wild-type and G $\alpha_{12/13}$ -deficient MEFs, but not G $\alpha_{q/11}$ -deficient cells,

showed stress-fiber formation upon toxin treatment, a result indicating Rho activation through $G\alpha_{q/11}$.

PaTox enters the cytosol from endosomes

In order to analyze the uptake of PaTox into target cells, we incubated RAW 264.7 cells with full-length PaTox in the presence of bafilomycin A1 or brefeldin A and analyzed PaTox uptake by deamidation of $G\alpha$ proteins (Supplementary Fig. 5c). Whereas the C-terminal toxin fragment PaTox^{G-D} could not enter the cell without the cell-delivery component PA, full-length PaTox entered the cytoplasm of the cell and deamidated $G\alpha$ proteins very efficiently. Bafilomycin A1 but not brefeldin A inhibited the toxin effect, thus indicating that PaTox translocation into the cytoplasm was dependent on the acidification of an early-endosomal compartment and did not succeed through Golgi retrograde trafficking to the endoplasmic reticulum, which would be affected by brefeldin A.

DISCUSSION

Here, we report on PaTox, a new toxin from *P. asymbiotica* that targets Rho proteins by tyrosine glycosylation and heterotrimeric G proteins by deamidation. We suggest that PaTox is a single-chain AB toxin with two catalytic domains at the C terminus and a receptor-translocation domain at the N terminus, and it probably enters host cells from early endosomes.

Rho as a target is shared by several bacterial protein toxins and effectors^{1,26}. *P. luminescens*, which is related to *P. asymbiotica*, produces a toxin complex (Tc) that modifies Rho proteins of insect target cells. The active component, TccC5, activates Rho proteins by ADP ribosylation at Q61 (or Q63)¹⁹. Notably, *P. asymbiotica* does not contain TccC5. However, PaTox is unique for *P. asymbiotica* and is not present in other *Phototribadus* species. Accordingly, we detected tyrosine GlcNAcylation only during *P. asymbiotica* infection of insect cells but not during *P. luminescens* infection. Whether PaTox is essential for infection in humans remains to be clarified.

Intriguingly, PaTox GlcNAcylates Rho proteins selectively at Y32 (or Y34). This unusual modification was highly specific with respect to the acceptor amino acid. Y32 (or Y34) is a highly conserved amino acid located in the switch I region of Rho proteins, a region crucial for regulation and binding to downstream effectors. GlcNAcylation of Y32 (or Y34) inhibits activation of Rho proteins by GEFs, blocks GAP binding and inhibits effector interaction. Consequently, Rho signaling is impaired, and this results in disassembly of the actin cytoskeleton and eventually in cell death. Notably, the same site, Y32 (or Y34), is adenylylated (AMPylated) by the *Histophilus somni* effector IbpA²⁷, and modification prevents effector interaction, thus indicating the pivotal functional role of this residue in Rho GTPases. Interestingly, the active GTP-bound conformation of Rho is the preferred substrate for PaTox-induced glycosylation. By contrast, the inactive GDP-bound form of RhoA is favored as a substrate for modification of T35 (or T37) by clostridial glucosylating toxins²⁸.

Glycosyltransferases are classified as inverting or retaining enzymes, depending on the stereochemical outcome of the transfer reaction at the anomeric glycosidic bond with respect to the donor substrate²⁹. Our ¹H-NMR analysis showed that PaTox is highly stereospecific and assigns PaTox to the family of retaining glycosyltransferases. Moreover, NMR measurements with RhoA revealed that changes caused by GlcNAcylation are restricted to Y34 only and do not alter the arrangement of the switch I region, thus suggesting that the attached GlcNAc residue impairs effector and regulator interaction, probably by steric hindrance. This is in contrast to the H-Ras and Rac glucosylating *Clostridium sordellii* lethal toxin, which

stabilizes the inactive GDP-bound conformation and thereby prevents effector interaction³⁰. The stereochemistry of the attached sugar is important to prevent sugar removal by endogenous stereoselective glycosidases. In the eukaryotic cytoplasm exists an O-GlcNAcase that is a specific β -glycosidase and is not able to hydrolyze α -glycosidic linkages³¹. Also, in lysosomes α -glycosidases (EC 3.2.1.50) are present. However, it is questionable whether they reach the cytoplasm. Nevertheless, it would be of interest to study whether they are able to cleave tyrosine-glycosylated substrates.

The crystal structure of PaTox^G revealed a unique GT-A structural fold, which is the smallest known for glycosyltransferase toxins, as PaTox^G lacks extending subdomains. Those subdomains have been shown to be crucial for Rho versus Ras recognition by clostridial glucosylating toxins (for example, *C. difficile* toxin B and *C. sordellii* lethal toxin)³². Therefore, we suggest that PaTox^G interacts with Rho in a distinct mode.

Mono-O-GlcNAcylation of serine and threonine residues in the nucleocytoplasm is a well-known mechanism mediated by O-GlcNAc transferase⁴. Tyrosine residues are known to become post-translationally modified by phosphorylation or sulfation, but attachment of a sugar onto a tyrosine hydroxyl group in eukaryotes has only been described for glycogenin. This enzyme synthesizes a maltosaccharide chain by autoglycosylation of a tyrosine in a stepwise reaction, and this initiates glycogen synthesis^{33,34}. It is intriguing that, besides bacterial glucosylating toxins, *P. asymbiotica* PaTox glycosyltransferase shares the highest structural similarities with glycogenin and uses mono-O-GlcNAcylation of tyrosine to control the activity of eukaryotic host GTPases. Recent genetic and O-glycoproteome analyses reported that tyrosine glycosylation may also exist in eukaryotic and prokaryotic glycoproteins. Whereas in prokaryotes a tyrosine-modifying O-oligosaccharyl protein transferase (*Paenibacillus alvei* WsfB) has been recently identified by Messner and colleagues³⁵, in eukaryotes tyrosine glycosyltransferases remain enigmatic^{36–37}. It appears that tyrosine glycosylation is an overlooked and rather unexplored modification.

We identified a deamidase domain downstream of the glycosyltransferase domain of PaTox, with similarity to SseI. Although the crystal structure of *Salmonella* SseI was shown to be very similar to PMT, enzyme activity or substrates of SseI remained enigmatic¹⁴. Here we show that the SseI-like domain of PaTox activates G_1 and $G_{q/11}$ by deamidation of a crucial glutamine residue involved in GTP hydrolysis of the G proteins. From our results, we speculate that *Salmonella* SseI is also a $G\alpha$ protein-deamidating effector, which might modulate host-cell migration in a $G_{q/11}$ - or G_1 -dependent manner³⁸. Because PaTox activates several heterotrimeric G proteins, the functional consequences of their activation are difficult to elucidate and require further analyses. However, it is intriguing that the preferred substrate of Rho inhibition by glucosylation is the GTP-loaded form of Rho. GDP-GTP exchange of RhoA might be triggered through signaling pathways mediated by the deamidation of $G\alpha_{q/11}$ (ref. 39).

Thus, the same toxin causes activation (through PaTox^D) and inactivation (through PaTox^G) of Rho proteins. Because glycosylation-induced inactivation dominates, it remains to be clarified whether these opposing actions occur in a defined spatiotemporal manner during host infection, similarly as reported for the activation and inactivation of Rho proteins by the *Salmonella* RhoGEF SopE and RhoGAP SptP, respectively⁴⁰, or bidirectionally, as in the regulation of Rab proteins by *Legionella* effectors⁴¹. In conclusion, PaTox is a new protein toxin that interferes with host-cell signaling by a specific tyrosine glycosylation of Rho proteins and by deamidation of heterotrimeric $G\alpha$ proteins. Our data open new perspectives in carbohydrate and bacterial-toxin research.

METHODS

Methods and any associated references are available in the [online version of the paper](#).

Accession codes. Coordinates and structural factors for the reported crystal structure have been deposited in the Protein Data Bank under accession code [4MIX](#).

Note: Any Supplementary Information and Source Data files are available in the [online version of the paper](#).

ACKNOWLEDGMENTS

We thank P. Gebhardt for technical assistance, P. Papatheodorou for discussions and U. Lanner for supporting MS analyses. We thank S. Offermanns (Max-Planck-Institute) for providing $G\alpha_{q11}$ - and $G\alpha_{12/13}$ -deficient MEFs, Y. Horiguchi (Osaka University) for the deamidation-specific antibody anti-G α QE (3G3) and A.E. Lang (University of Freiburg) for providing anthrax protective antigen. The plasmids pGEX4T1-LARG (residues 766–1138) and pGEX4T1-PDZ-RhoGEF (residues 712–1081) were kindly provided by M. Reza Ahmadian (University Düsselldorf). We thank the BM14 (European Synchrotron Radiation Facility) and PXI (Swiss Light Source) beamline staff for their support. This work was supported by the Deutsche Forschungsgemeinschaft Collaborative Research Center 746 (K.A., J.H.C.O. and C.H.), Deutsche Forschungsgemeinschaft AK6/22-1 (K.A.) and the Excellence Initiative of the German Federal and State Governments EXC 294 BIOS (K.A., C.H. and B.W.).

AUTHOR CONTRIBUTIONS

T.J. designed the study, performed experiments, analyzed the data and wrote the paper; K.A. designed the study, analyzed data and wrote the paper; K.E.B. and M. Steinemann collected data; J.H.C.O. designed the study; E.H. and B.W. performed MS analyses; X.B., C.W. and C.H. performed X-ray analysis; M. Spoerner and H.R.K. performed NMR analysis; and all authors discussed the results and commented on the manuscript.

COMPETING FINANCIAL INTERESTS

The authors declare no competing financial interests.

Reprints and permissions information is available online at <http://www.nature.com/reprints/index.html>.

- Aktorics, K. Bacterial protein toxins that modify host regulatory GTPases. *Nat. Rev. Microbiol.* **9**, 487–498 (2011).
- Belyi, Y., Jank, T. & Aktories, K. Effector glycosyltransferases in *Legionella*. *Front. Microbiol.* **2**, 76 (2011).
- Kelly, C.P. & LaMont, J.T. *Clostridium difficile*: more difficult than ever. *N. Engl. J. Med.* **359**, 1932–1940 (2008).
- Hart, G.W. Dynamic O-GlcNAcylation of nuclear and cytoskeletal proteins. *Annu. Rev. Biochem.* **66**, 315–335 (1997).
- Gerrard, J., Waterfield, N., Vohra, R. & French-Constant, R. Human infection with *Photorhabdus asymbiotica*: an emerging bacterial pathogen. *Microbes Infect.* **6**, 229–237 (2004).
- Waterfield, N.R., Ciche, T. & Clarke, D. *Photorhabdus* and a host of hosts. *Annu. Rev. Microbiol.* **63**, 557–574 (2009).
- French-Constant, R. *et al.* *Photorhabdus*: towards a functional genomic analysis of a symbiont and pathogen. *FEMS Microbiol. Rev.* **26**, 433–456 (2003).
- Farmer, J.J. III *et al.* *Xenorhabdus luminescens* (DNA hybridization group 5) from human clinical specimens. *J. Clin. Microbiol.* **27**, 1594–1600 (1989).
- Peel, M.M. *et al.* Isolation, identification, and molecular characterization of strains of *Photorhabdus luminescens* from infected humans in Australia. *J. Clin. Microbiol.* **37**, 3647–3653 (1999).
- Gerrard, J.G. *et al.* Nematode symbiont for *Photorhabdus asymbiotica*. *Emerg. Infect. Dis.* **12**, 1562–1564 (2006).
- Wilkinson, P. *et al.* Comparative genomics of the emerging human pathogen *Photorhabdus asymbiotica* with the insect pathogen *Photorhabdus luminescens*. *BMC Genomics* **10**, 302 (2009).
- McLaughlin, L.M. *et al.* The *Salmonella* SPI2 effector Ssel mediates long-term systemic infection by modulating host cell migration. *PLoS Pathog.* **5**, e1000671 (2009).
- Worley, M.J., Nieman, G.S., Geddes, K. & Heffron, F. *Salmonella typhimurium* disseminates within its host by manipulating the motility of infected cells. *Proc. Natl. Acad. Sci. USA* **103**, 17915–17920 (2006).
- Bhaskaran, S.S. & Stebbins, C.E. Structure of the catalytic domain of the *Salmonella* virulence factor Ssel. *Acta Crystallogr. D Biol. Crystallogr.* **68**, 1613–1621 (2012).
- Wiggins, C.A.R. & Munro, S. Activity of the yeast *MNN1* α -1,3-mannosyltransferase requires a motif conserved in many other families of glycosyltransferases. *Proc. Natl. Acad. Sci. USA* **95**, 7945–7950 (1998).
- Viisidou, I. *et al.* *Drosophila* embryos as model systems for monitoring bacterial infection in real time. *PLoS Pathog.* **5**, e1000518 (2009).
- Silva, C.P. *et al.* Bacterial infection of a model insect: *Photorhabdus luminescens* and *Manduca sexta*. *Cell Microbiol.* **4**, 329–339 (2002).
- Blanke, S.R., Milne, J.C., Benson, E.L. & Collier, R.J. Fused polycationic peptide mediates delivery of diphtheria toxin A chain to the cytosol in the presence of anthrax protective antigen. *Proc. Natl. Acad. Sci. USA* **93**, 8437–8442 (1996).
- Lang, A.E. *et al.* *Photorhabdus luminescens* toxins ADP-ribosylate actin and RhoA to force actin clustering. *Science* **327**, 1139–1142 (2010).
- Just, I. *et al.* Glucosylation of Rho proteins by *Clostridium difficile* toxin B. *Nature* **375**, 500–503 (1995).
- Jaffe, A.B. & Hall, A. Rho GTPases: biochemistry and biology. *Annu. Rev. Cell Dev. Biol.* **21**, 247–269 (2005).
- Flatau, G. *et al.* Toxin-induced activation of the G protein p21 Rho by deamidation of glutamine. *Nature* **387**, 729–733 (1997).
- Orth, J.H. *et al.* *Pasteurella multocida* toxin activation of heterotrimeric G proteins by deamidation. *Proc. Natl. Acad. Sci. USA* **106**, 7179–7184 (2009).
- Kamitani, S. *et al.* Enzymatic actions of *Pasteurella multocida* toxin detected by monoclonal antibodies recognizing the deamidated α subunit of the heterotrimeric GTPase G_q . *FEBS J.* **278**, 2702–2712 (2011).
- Tesmer, J.J., Berman, D.M., Gilman, A.G. & Sprang, S.R. Structure of RGS4 bound to AlF_4^- -activated G_{i1} : stabilization of the transition state for GTP hydrolysis. *Cell* **89**, 251–261 (1997).
- Visvikis, O., Maddugoda, M.P. & Lemichez, E. Direct modifications of Rho proteins: deconstructing GTPase regulation. *Biol. Cell* **102**, 377–389 (2010).
- Worby, C.A. *et al.* The fic domain: regulation of cell signaling by adenylation. *Mol. Cell* **34**, 93–103 (2009).
- Herrmann, C., Ahmadian, M.R., Hofmann, F. & Just, I. Functional consequences of monoglucosylation of H-Ras at effector domain amino acid threonine-35. *J. Biol. Chem.* **273**, 16134–16139 (1998).
- Coutinho, P.M., Deleury, E., Davies, G.J. & Henrissat, B. An evolving hierarchical family classification for glycosyltransferases. *J. Mol. Biol.* **328**, 307–317 (2003).
- Vetter, I.R., Hofmann, F., Wohlgemuth, S., Herrmann, C. & Just, I. Structural consequences of mono-glucosylation of Ha-Ras by *Clostridium sordellii* lethal toxin. *J. Mol. Biol.* **301**, 1091–1095 (2000).
- Hanover, J.A., Krause, M.W. & Love, D.C. Bittersweet memories: linking metabolism to epigenetics through O-GlcNAcylation. *Nat. Rev. Mol. Cell Biol.* **13**, 312–321 (2012).
- Jank, T., Giesemann, T. & Aktories, K. *Clostridium difficile* glycosyltransferase toxin B: essential amino acids for substrate-binding. *J. Biol. Chem.* **282**, 35222–35231 (2007).
- Smythe, C., Caudwell, F.B., Ferguson, M. & Cohen, P. Isolation and structural analysis of a peptide containing the novel tyrosyl-glucose linkage in glycogenin. *EMBO J.* **7**, 2681–2686 (1988).
- Chaikwad, A. *et al.* Conformational plasticity of glycogenin and its maltosaccharide substrate during glycogen biogenesis. *Proc. Natl. Acad. Sci. USA* **108**, 21028–21033 (2011).
- Zarschler, K. *et al.* Protein tyrosine O-glycosylation: a rather unexplored prokaryotic glycosylation system. *Glycobiology* **20**, 787–798 (2010).
- Steenfot, C. *et al.* Mining the O-glycoproteome using zinc-finger nuclease-glycoengineered SimpleCell lines. *Nat. Methods* **8**, 977–982 (2011).
- Halim, A. *et al.* Site-specific characterization of threonine, serine, and tyrosine glycosylations of amyloid precursor protein/amyloid β -peptides in human cerebrospinal fluid. *Proc. Natl. Acad. Sci. USA* **108**, 11848–11853 (2011).
- Cotton, M. & Claing, A. G protein-coupled receptors stimulation and the control of cell migration. *Cell Signal.* **21**, 1045–1053 (2009).
- Lutz, S. *et al.* Structure of $G\alpha_q$ -p63RhoGEF-RhoA complex reveals a pathway for the activation of RhoA by GPCRs. *Science* **318**, 1923–1927 (2007).
- Schlumberger, M.C. & Hardt, W.D. Triggered phagocytosis by *Salmonella*: bacterial molecular mimicry of RhoGTPase activation/deactivation. *Curr. Top. Microbiol. Immunol.* **291**, 29–42 (2005).
- Goody, R.S. *et al.* The versatile *Legionella* effector protein DrrA. *Commun. Integr. Biol.* **4**, 72–74 (2011).

ONLINE METHODS

Materials, bacterial strains and plasmids. DNA-modifying enzymes were from Fermentas (St. Leon-Rot, Germany), Phusion High-Fidelity DNA Polymerase from New England Biolabs (Ipswich, MA) and PfuUltra HF DNA Polymerase from Stratagene (Waldbronn, Germany). UDP-[¹⁴C]glucose and UDP-[¹⁴C]N-acetylglucosamine were from Biotrend (Cologne, Germany). UDP-[¹⁴C]galactose was from PerkinElmer Life Sciences (Rodgau, Germany). 2'(3')-O-(N-methylanthraniloyl) guanosine 5'-diphosphate (mant-GDP) and mant-guanosine 5'-[β , γ -imido]triphosphate (mant-GppNHp) were from Jena Bioscience (Jena, Germany). The pET28a vector was from Novagen (Madison, WI), and pGEX-4T1 and pGEX-4T3 were from GE Healthcare (Freiburg, Germany). *P. asymbiotica* subsp. *asymbiotica* (ATCC 43950) and *P. luminescens* subsp. *laumondii* (DSM 15195) were from the German Collection of Microorganisms and Cell Cultures (DSMZ) and were cultivated in CASO bouillon at 28 °C. *E. coli* TG1 was used for general cloning and protein expression of pGEX constructs. *E. coli* BL21 (DE3) CodonPlus (Stratagene) was used for protein expression of pET constructs. Toxin B was prepared from *C. difficile* supernatants as described⁴². Recombinant GTP-binding proteins and the glucosyltransferase domain of *C. difficile* toxin B were prepared as described earlier³². The plasmids pGEX4T1-LARG (residues 766–1138) and pGEX4T1-PDZ-RhoGEF (residues 712–1081) were kindly provided by M. Reza Ahmadian (University of Düsseldorf). All other reagents were of analytical grade and purchased from commercial sources.

Antibodies. Anti-RhoA (26C4, dilution 1:400) and anti-G α_q (sc-392, dilution 1:2,000)²⁴ antibodies were from Santa Cruz (California, USA), anti-Rac1 (Mab 102, dilution 1:5,000) from BD Bioscience (Heidelberg, Germany), anti-Rac1 (23A8, dilution 1:2,500) from Millipore (Schwalbach, Germany), anti-Cdc42 (17-299, 1:500) from Upstate and anti-GAPDH (6C5, dilution 1:20,000) antibody from Millipore. Anti-GST (27-4577-01, dilution 1:2,000) was from GE Healthcare and horseradish peroxidase-linked anti-mouse antibody from Rockland Immunochemicals (cat. no. 610-703-124, dilution 1:3,000). Antibody specifications are on manufacturer's website. Deamidation-specific anti-Gq QE (3G3) antibody²⁴ (dilution 1:250) was kindly provided by Y. Horiguchi (Osaka University).

Cloning of genes for bacterial expression. The gene PaTox (PAU_02230) and the fragments PaTox^G and PaTox^{G-D} were amplified with Phusion DNA polymerase from the genomic DNA of *P. asymbiotica* (ATCC 43950) with oligonucleotide primers with additional restriction sites for BamHI and SalI (**Supplementary Table 3**). The genes were ligated into a predigested pET28a vector with an introduced tobacco etch virus (TEV) protease cleavage site. QuikChange Kit (Stratagene, La Jolla, CA) in combination with PfuUltra HF DNA polymerase was used for the replacement of one to three nucleotides, using the oligonucleotides shown in **Supplementary Table 3**. All sequences of corresponding plasmids were confirmed by sequencing (GATC Inc., Konstanz, Germany).

Recombinant-protein expression. *E. coli* BL21* CodonPlus cells (Stratagene) transformed with the desired plasmids were grown in LB medium supplemented with the corresponding antibiotics on a shaker at 37 °C until A₆₀₀ = 0.8. Protein expression from the pET28-based plasmids was induced by 1 mM isopropyl- β -D-thiogalactopyranoside (IPTG) (Roth, Karlsruhe, Germany) for 4–5 h at 22 °C, and pGEX-based expression was induced with 0.2 mM IPTG at 37 °C for 6 h. Bacterial cells were harvested by centrifugation at 6,000g for 15 min, resuspended in lysis buffer (50 mM Tris-HCl, pH 7.4, 150 mM NaCl, 25 mM imidazole, 30 μ g/ml DNase I, 1 mM β -mercaptoethanol, and protease-inhibitor cocktail (Roche)) and lysed by French press or ultrasonic treatment. The cleared lysate was subjected to chromatography on a glutathione-Sepharose or nickel-equilibrated chelating Sepharose Fast Flow column (GE Healthcare) according to the manufacturer's instructions. Bound proteins were eluted with 10 mM reduced glutathione, 0.5 M imidazole, thrombin treatment, or TEV protease treatment, depending on the construct used. Thrombin was removed by binding to benzamidine-Sepharose (GE Healthcare) and His-TEV by Ni²⁺-affinity chromatography. Further purification and removal of protein impurities or small-molecular-weight components such as reduced GSH, EDTA, and labeled and unlabeled nucleotides or analogs was achieved by size-exclusion chromatography with Superdex 75 or Superdex 200 (each 10/300) columns. For crystallization, selenomethionine-labeled PaTox^G (residues 2115–2449) was expressed and purified as His-tagged

protein with the method of Studier⁴³. After removal of the His tag by TEV-protease treatment, PaTox^G was additionally purified by cation-exchange chromatography (Resource S, GE Healthcare) and size-exclusion chromatography (Superdex 75, GE Healthcare).

Cell culture. HeLa (ATCC CCL-2), RAW 264.7 (ATCC TIB-71) and J774 (ATCC TIB-67) cells were cultured in Dulbecco's modified Eagle's medium (DMEM) supplemented with 10% FCS, 1% nonessential amino acids, 4 mM penicillin, 4 mM streptomycin, and 1% sodium pyruvate (Biochrom, Berlin, Germany). Cells were cultivated in a humidified atmosphere of 5% CO₂ at 37 °C. Where necessary, cells were starved overnight in DMEM without FCS. *Spodoptera frugiperda* Sf9 cells (ATCC CRL-1711) were cultivated in Grace's insect medium (GIM) at 28 °C. For intoxication of cells, GST-CNFy (400 ng/ml), PMT (150 ng/ml) native full-length *C. difficile* toxin B (1 ng/ml), or a combination of *Bacillus anthracis* protective antigen (PA, 0.5 μ g/ml) and PaTox-fragments (370 ng/ml), were applied into the medium and incubated for 4 h if not otherwise stated.

Actin staining. HeLa cells grown on glass coverslips were washed with PBS, fixed with 4% formaldehyde in PBS and permeabilized with 0.15% (v/v) Triton X-100 in PBS for 10 min at room temperature. Subsequently, the cells were incubated with TRITC-conjugated phalloidin and washed again with PBS. Cells were embedded with Mowiol supplemented with 1,4-diazobicyclo[2.2.2]octane (Sigma) and analyzed by fluorescence microscopy with an Axiophot system (Zeiss, Oberkochen, Germany), and data were processed by Metamorph 7.0 (Universal Imaging, Downingtown, PA).

G. mellonella injection. Latest-instar *G. mellonella* larvae were selected by similar size and absence of any gray markings for reproducible results. Larvae were randomly chosen, chilled on ice for 5 min and surface-disinfected with 70% ethanol. A microsyringe with a 26-gauge needle was used to inject 10 μ l PaTox toxin or PaTox(NxN) solution (50 ng per larva), into the hemocoel through the last left proleg. Control insects were injected with 10 μ l PBS or left untreated. Two larvae from the toxin-injected group and one from the mutant group were excluded from the analysis because the injection had failed. Larvae from each replicate were placed onto Greiner six-well plates (one larva per well) and incubated in the dark at 28 °C for 88 h. Loss of larvae reaction upon poking and intense blackening due to melanization were used as indication of death. Differences in survival were analyzed by the Kaplan–Meier method with SigmaPlot 10.0 (Systat Software). Expecting that toxin injection would result in death of all animals, we chose a sample size of around 20. Control sample size was chosen on the basis of previous experiments showing no toxicity. Outcome assessment was performed by a person not involved in injection of larvae.

Hydrolysis of UDP sugars by PaTox. UDP-sugar hydrolysis was measured as described earlier for the glucosyltransferase toxin B from *C. difficile*³². PaTox^G (100 nM) was incubated with 10 μ M UDP-[¹⁴C]sugars in a buffer containing 50 mM HEPES, pH 7.5, 2 mM MgCl₂ and 1 mM MnCl₂. Total volume was 10 μ l. After incubation for 15 min at 30 °C, samples of 800 nl were taken and subjected to polyethyleneimine (PEI)-cellulose thin-layer chromatography (Merck, Darmstadt, Germany) with 0.2 mM LiCl as mobile phase to separate the hydrolyzed sugar from intact UDP sugar. The plates were dried and analyzed by Phosphorimager. Quantification was carried out with ImageQuant (GE Healthcare).

Glycosylation reaction. Recombinant PaTox^G (1 nM or 10 nM in **Fig. 2d,e**; 100 nM in **Fig. 2f**) or the glucosyltransferase domain of *C. difficile* toxin B (1 nM) were incubated with 10 μ M UDP-[¹⁴C]N-acetylglucosamine or UDP-[¹⁴C]glucose, respectively, in a buffer, containing 50 mM HEPES, pH 7.4, 2 mM MgCl₂, and 1 mM MnCl₂ for 30 min at 30 °C in the presence of recombinant GST-tagged GTP-binding proteins (2 μ M, 4 μ M in **Fig. 2**) or cell lysate as described previously³². 1 μ g bovine serum albumin was added in reactions determining substrate specificity. In the case of toxin B, potassium chloride was added to a final concentration of 100 mM. Total volume was 20 μ l. Labeled proteins were analyzed by SDS-PAGE and phosphorimaging. For quantitative modification, GST-RhoA bound to glutathione-Sepharose beads was modified with PaTox^G (10 nM) and UDP-GlcNAc (100 μ M) or toxin B (10 nM) with UDP-glucose (100 μ M). Beads were extensively washed with glycosylation buffer, and RhoA was eluted by thrombin cleavage in buffer C (10 mM TEA, pH 7.5, 150 mM NaCl, and 2.5 mM MgCl₂).

Thrombin was removed by the incubation with benzamidine-Sepharose. Complete glycosylation was confirmed by a second *in vitro* glycosylation reaction. All glycosylation reactions were repeated three times.

Mass spectrometric analysis. Glycosylation of RhoA, Rac1 and Cdc42 (5 μ g each) was performed with PaTox^G (100 nM) in the presence of UDP-GlcNAc (1 mM) for 30 min at 30 °C in glycosylation buffer. Deamidation of GST-G α_{i2} (2 μ g) was performed by incubation with PaTox^{G-S} (100 nM) for 1 h at 30 °C in a buffer containing 50 mM HEPES, pH 7.4, 50 mM NaCl, 5 mM MgCl₂. Afterwards, the samples were reduced with 50 mM DTT and alkylated with 120 mM iodoacetamide before SDS-PAGE. Excised gel bands were destained with 30% acetonitrile (ACN), shrunk with 100% ACN, and dried in a vacuum concentrator. Subsequently, protein digestion with thermolysin (Rho proteins) was performed for 3 h at 60 °C in 0.1 M NH₄HCO₃, pH 8, and digestion of GST-G α_{i2} with trypsin was performed overnight at 37 °C in 0.1 M NH₄HCO₃, pH 8. Approximately 0.1 μ g of protease per gel band was used. Peptides were extracted from the gel matrix with 5% formic acid and subsequently analyzed by LC-MS on a Q-TOF mass spectrometer (Agilent 6520, Agilent Technologies) coupled to a 1200 Agilent nanoflow system through a HPLC-Chip cube electrospray ionization interface. Peptides were separated on a HPLC-Chip with an analytical column of 75 μ m i.d. and 150 mm length and a 40-nl trap column, both packed with Zorbax 300SB C-18 (5- μ m particle size). Starting with 3% ACN, a linear gradient with 1%/min at a flow rate of 300 nl/min was applied. The Q-TOF instrument was operated in the 2-GHz extended dynamic range mode, and MS spectra were acquired in the *m/z* range between 50 and 3,000. For MS/MS analyses, the instrument was operated in the data-dependent acquisition mode. After a survey MS scan (four spectra per second), a maximum of three multiple-charged peptides were consecutively selected for MS/MS experiments (two spectra per second). Internal mass calibration was applied. Mascot Distiller 2.4.2 was used for raw-data processing and for generating peak lists, essentially with standard settings for the Agilent Q-TOF instrument. Mascot Server 2.3 was used for searches in the SwissProt protein database with the following parameters: peptide mass tolerance, 50 p.p.m.; MS/MS mass tolerance, 0.05 Da; enzyme, no specificity; variable modifications, carbamidomethyl (C), Gln \rightarrow pyroGlu (N-term. Q), oxidation (M) and HexNAc (STY).

Effector- and GAP-binding assay. The Rho-binding region (RBD) of Rhotekin (amino acids 1–90), the CRIB domain of PAK (amino acids 56–272), and p50RhoGAP were expressed as GST-fusion proteins in *E. coli* BL21 and purified by affinity chromatography with glutathione-Sepharose beads (GE Healthcare). HeLa cells were treated with a combination of PA (0.5 μ g/ml) and *Photorhabdus* glucosyltransferase fragments (100 ng/ml), *C. difficile* toxin B (1 ng/ml) or GST-CNF γ (400 ng/ml) for 12 h. Then cells were stimulated with fresh FCS for 10 min at 37 °C. Subsequently, cells were lysed in ice-cold buffer A (50 mM Tris, pH 7.4, 100 mM NaCl, 1% NP-40, 10% glycerol, 2 mM MgCl₂ and 1 mM PMSF), and cellular debris was removed by centrifugation (30 min, 14,000 r.p.m.). A fraction of the cleared lysates (50 μ g of total protein) was analyzed by immunoblotting to detect total amounts of the respective GTPases and GAPDH as a loading control. The lysates were incubated for 60 min at 4 °C with GST-Rhotekin (RBD), GST-PAK (CRIB domain) or GST-p50GAP immobilized on glutathione-Sepharose beads. The beads were precipitated and washed with buffer A. Finally, proteins were subjected to SDS-PAGE and transferred onto PVDF membranes, and GTPases were detected by specific antibodies and horseradish peroxidase-linked secondary antibodies.

For *in vitro* effector-pulldown experiments, recombinant wild-type and glycosylated RhoA, Rac1, and Cdc42 (2 μ g) were loaded with the indicated non-hydrolyzable nucleotides GTP γ S or GDP β S (each 200 μ M final concentration) by incubation in buffer C (10 mM TEA, pH 7.5, 150 mM NaCl, and 2.5 mM MgCl₂) for 30 min at 37 °C. Samples were diluted and incubated for 20 min at 4 °C with GST-Rhotekin (RBD), GST-PAK (CRIB domain), or GST-RhoGAP immobilized on glutathione-Sepharose beads. Beads were washed and precipitated proteins analyzed by western blotting. All experiments were repeated three times.

Filter-binding assay for GAP-stimulated GTPase activity. Toxin-treated or control GTPases (2.2 μ M) were loaded with [γ -³²P]GTP (100 μ M) for 5 min at 37 °C in loading buffer (50 mM Tris-HCl, pH 7.5, 10 mM EDTA, and 5 mM DTT). MgCl₂ (25 mM, final concentration) and unlabeled GTP (2 mM final concentration)

were added. GTPase activity was measured at 25 °C. GAP stimulation was performed by the addition of the 30-kDa active fragment of p50RhoGAP (216 nM final concentration). At the indicated time points, proteins were collected by filtration through wet 0.22- μ m nitrocellulose filter discs. The filters were washed three times with ice-cold buffer A (50 mM Tris-HCl, pH 7.5, 50 mM NaCl, and 5 mM MgCl₂), and protein-bound [γ -³²P]GTP was quantified by liquid scintillation counting.

Mant-GDP and mant-GppNHp binding. The measurements were carried out on a LS50B spectrofluorometer from PerkinElmer at 37 °C. The nucleotide exchange of RhoA was measured over time as the increase in fluorescence intensity at $\lambda_{em} = 444$ nm ($\lambda_{ex} = 360$ nm) of mant-nucleotides upon binding to RhoA. Mant-GDP or mant-GppNHp (1 μ M) was incubated with RhoA (0.5 μ M) in degassed buffer C (10 mM TEA, pH 7.5, 150 mM NaCl, and 2.5 mM MgCl₂). The samples were excited in a cycle of 1 min for 1 s. Exponential fitting of the data was done with SigmaPlot 10.0.

Measurements of G-nucleotide exchange reactions. Preglycosylated RhoA (0.5 μ M) and wild-type RhoA (0.5 μ M) were incubated with mant-GDP (1 μ M) in degassed buffer C at 20 °C. After 5 min, GEFs leukemia-associated RhoGEF (LARG), PDZ-RhoGEF or p47-LBC RhoGEF were added to a final concentration of 200 nM and incubated for the indicated time periods. Fluorescence was measured with an LS50B spectrofluorometer at $\lambda_{em} = 460$ nm ($\lambda_{ex} = 360$). Each experiment was repeated twice.

Crystallization. SeMet-derivatized PaTox^G (amino acids 2115–2449) was crystallized by the sitting-drop vapor-diffusion method at 18 °C. Protein (10–15 mg/ml in 10 mM Tris-HCl, pH 7.4, and 150 mM NaCl) was mixed 1:1 with reservoir solution (100 mM Tris-HCl, pH 8.5, 500 mM NaCl and 20% PEG 3350). For UDP-GlcNAc binding, crystals were soaked for 10 min with 5 mM UDP-GlcNAc and 5 mM CaCl₂. 20% ethylene glycol was used for cryoprotection.

Data collection and refinement. Diffraction data were collected at 100 K on beamlines PXI of the Swiss Light Source (SLS) and BM14 of the European Synchrotron Radiation Facility (ESRF), processed with XDS⁴⁴ or MOSFLM⁴⁵ and integrated with SCALA⁴⁶. Structure solution was performed by SAD with PHENIX AutoSol⁴⁷ to identify selenomethionine positions. An initial model for structure refinement was obtained from PHENIX AutoBuild⁴⁸. The final model was obtained after several alternated cycles of model building with COOT⁴⁹ and REFMAC⁵⁰ from the CCP4 suite⁵¹. Quality of the structure was checked with PROCHECK⁵² and MolProbity⁵³ and resulted in 98.7% of the residues in the most-favored and 1.3% in the additionally allowed regions of the Ramachandran plot. Figures were prepared with PyMOL (<http://www.pymol.org/>). Data collection and refinement statistics are in **Table 1**.

¹H-NMR analysis. The samples contained 0.7 mM RhoA-Mg²⁺-GDP in d₁₁ Tris-HCl, pH 7.1, 30 mM NaCl, 10 mM MgCl₂, and 0.2 mM DSS in D₂O. ¹H 1D NOESY experiments were performed with a mixing time of 10 ms and solvent presaturation during relaxation delay and mixing time. A spoil gradient was applied during mixing time. Homonuclear ¹H 2D NOESY and TOCSY spectra were recorded with 4,096 data points in the *t*₂ dimension and 1,024 real free induction decays in the *t*₁ dimension. NOESY spectra were acquired with mixing time of 150 ms and water suppression by presaturation during relaxation delay and mixing time. TOCSY spectra were performed with a MLEV17 sequence and a spinlock time of 60 ms. The water signal was suppressed by selective excitation with 3–9–19 pulse with defocusing gradients⁵⁴. Measurements were performed in a 5-mm tube within a Bruker Avance 600 NMR spectrometer equipped with a TXI-Cryo probe. Proton chemical shifts were referenced to 4,4-dimethyl-4-silapentane-1-sulfonic acid (DSS) as internal standard. To investigate protein modification, we added 2 mM UDP-GlcNAc and 2.5 nM PaTox^G to 1 mM RhoA-Mg²⁺-GDP in buffer mentioned above. The reaction was followed by a series of ¹H 1D NOESY spectra at 298 K. After the reaction was completed, the protein was applied to size-exclusion chromatography (NAP 5 column) in the same buffer to remove most of the free nucleotide. From this sample, 1D as well as 2D TOCSY and NOESY spectra were recorded at 298 K. Afterwards the modified and native protein was denatured in the presence of 6 M urea, and the same set of spectra were recorded at 323 K. The resonances of the ring protons of Y34 were assigned with classical

methods from their cross-peak patterns in 2D TOCSY and 2D NOESY spectra recorded in D₂O. **Figure 5a** shows that selectively one tyrosine cross-peak pattern is influenced by the modification. NOESY cross-peaks from the H^δ to the H^β and H^α allow the identification of the corresponding spin systems, supported by H^β-H^α TOCSY cross-peaks. In unmodified RhoA, the corresponding chemical-shift value in the native protein of the H^α shift corresponds exactly to that reported⁵⁵ for Y34. In the modified protein, the corresponding values are 4.43 p.p.m. (H^α), 2.98 p.p.m. and 2.92 p.p.m. (H^β), 7.12 p.p.m. (H^δ) and 7.00 p.p.m. (H^ε). In the modified protein, cross-peaks from H^ε of Y34 to the H1' of the bound GlcNAc are visible (**Fig. 5b**). The chemical shift of the H1' of the GlcNAc bound to tyrosine (5.49 p.p.m) is typical for an α-anomer (**Fig. 5b,c**). The data were resolution-enhanced by a Lorentzian-to-Gaussian filtering. A fit of the spectrum with a Gaussian function provides a *J*-coupling value of 3.4 ± 0.5 Hz (the error corresponds to the digital resolution of the free induced decay) that is also in the typical range for an α-anomer⁵⁶. In the presence of 6 M urea and at a temperature of 323 K, RhoA is denatured, and the chemical shift of H1' of GlcNAc bound is 5.47 p.p.m., thus indicating that it occurs in the α-configuration.

Original images of gels, autoradiographs and blots used in this study can be found in **Supplementary Figures 6** and **7**.

42. Just, I., Selzer, J., Hofmann, F. & Aktories, K. in *Bacterial Toxins: Tools in Cell Biology and Pharmacology* (ed. Aktories, K.) 159–168 (Chapman & Hall, Weinheim, 1997).
43. Studier, F.W. Protein production by auto-induction in high density shaking cultures. *Protein Expr. Purif.* **41**, 207–234 (2005).
44. Kabsch, W. XDS. *Acta Crystallogr. D Biol. Crystallogr.* **66**, 125–132 (2010).
45. Leslie, A. & Powell, H. in *Evolving Methods for Macromolecular Crystallography* (eds. Read, R. & Sussman, J.) 41–51 (Springer, Netherlands, 2007).
46. Evans, P. Scaling and assessment of data quality. *Acta Crystallogr. D Biol. Crystallogr.* **62**, 72–82 (2006).
47. Terwilliger, T.C. *et al.* Decision-making in structure solution using Bayesian estimates of map quality: the PHENIX AutoSol wizard. *Acta Crystallogr. D Biol. Crystallogr.* **65**, 582–601 (2009).
48. Terwilliger, T.C. *et al.* Iterative model building, structure refinement and density modification with the PHENIX AutoBuild wizard. *Acta Crystallogr. D Biol. Crystallogr.* **64**, 61–69 (2008).
49. Emsley, P. & Cowtan, K. Coot: model-building tools for molecular graphics. *Acta Crystallogr. D Biol. Crystallogr.* **60**, 2126–2132 (2004).
50. Murshudov, G.N. *et al.* REFMAC5 for the refinement of macromolecular crystal structures. *Acta Crystallogr. D Biol. Crystallogr.* **67**, 355–367 (2011).
51. Winn, M.D. *et al.* Overview of the CCP4 suite and current developments. *Acta Crystallogr. D Biol. Crystallogr.* **67**, 235–242 (2011).
52. Laskowski, R.A., MacArthur, M.W., Moss, D.S. & Thornton, J.M. PROCHECK: a program to check the stereochemical quality of protein structures. *J. Appl. Crystallogr.* **26**, 283–291 (1993).
53. Chen, V.B. *et al.* MolProbity: all-atom structure validation for macromolecular crystallography. *Acta Crystallogr. D Biol. Crystallogr.* **66**, 12–21 (2010).
54. Sklenar, V., Piotto, M., Leppik, R. & Saudek, V. Gradient-tailored water suppression for ¹H-¹⁵N HSQC experiments optimized to retain full sensitivity. *J. Magn. Reson. A* **102**, 241–245 (1993).
55. Gasmi-Seabrook, G.M. *et al.* Real-time NMR study of guanine nucleotide exchange and activation of RhoA by PDZ-RhoGEF. *J. Biol. Chem.* **285**, 5137–5145 (2010).
56. Friebolin, H. *Basic One- and Two-Dimensional NMR Spectroscopy* (Wiley-VCH, Weinheim, 2010).